8-31-2021

Investigation of Environmental-Friendly, Membraneless Hydrogen Peroxide Fuel Cells

Bao Nguyen
Portland State University

Investigation of Environmental-Friendly, Membraneless Hydrogen Peroxide Fuel Cells

by

Bao Nguyen

A thesis submitted in fulfillment of the
requirements for the degree of

Master of Science
in
Physics

Thesis Committee:
Raj Solanki, Chair
Gary Goncher
Shankar Rananavare

Portland State University
2021

Abstract

Human-induced climate change is one of the biggest threats to humanity in the 21^{st} century. This is caused by the increase in greenhouse gas concentrations in the Earth's atmosphere. The burning of fossil fuels is the primary cause of climate change. This problem can be addressed by replacing fossil fuels with fuel sources that have clean by-products and are cost-effective. For the last few decades, hydrogen (H_2) has been extensively studied as an alternative to carbon-based fossil fuels. Currently, H_2 still has many shortcomings for commercial applications. The photocatalytic production of H_2 still suffers from extremely low efficiency. Furthermore, H_2 has low volumetric energy density and the current catalytic materials for H_2 are scarce and expensive. Alternatively, hydrogen peroxide (H_2O_2) is an environmental-friendly and high-energy carrier that can be utilized in fuel cell technologies to combat climate change. Recently, H_2O_2 has been successfully used as both a fuel and an oxidant in an acidic single compartment membraneless fuel cells (SCMHFC) where water and oxygen are the by-products. One of the challenges limiting SCMHFC is the low electric power generation. Hence, much effort has gone into finding suitable catalysts to improve the power density of SCMHFC. In this study, low cost and environmentally friendly catalysts have been investigated to product high power density SCMHFC. Among the catalysts examined were metallophthalocyanine complexes (FePc,CoPc, CuPc), iron nitride ($Fe_{x=2,4}N$), coblamin (Vitamin B12), modified cobalt-prussian blue complex (Co-Fe PB), and Fe/Fe_3C as the cathode materials and nickel as the anode. Electrochemical properties of these fuel cells were characterized. The open circuit potentials of the catalysts examined

ranged from 0.48 V to 0.68 V, with the highest power density of 2.8 $mW \cdot cm^{-2}$ with FePc, which is suitable for powering portable microelectronic devices.

Acknowledgements

I would like to express my sincere gratitude to my thesis adviser Professor Raj Solanki for not only the research opportunity, but also for his valuable guidance, encouragement, and incredible support. I would also like to gratefully thank my thesis committee members Professor Gary Goncher and Professor Shankar Rananavare for their time, patience, meaningful discussions, and their help with the thesis writing process.

I would like to thank Professor Erik Sanchez and Abdulsalam Almutairi for their endless encouragement and support since the beginning of the Master's program. I would also like to express my appreciation to Neal Kuperman, Warren Hollinshead, Jeff Black, Chris Halseth, Cristal Vann, Laurie Tull, Reina Tan, and Kim Doty-Harris for all of their help at Portland State University.

I would like to thank my former teammates at Thermo Fisher Scientific for their moral and financial supports.

Lastly, I would like to express my deepest gratitude to my parents Dai Tran and Dung Truong for their wisdom and sacrifices, Nghia Le, Minh Truong, Thanos Nguyen, and Boba Le for their moral support and encouragement.

Contents

List of Figures

List of Tables

Chapter 1

Introduction

1.1 Climate Change and Energy Crisis

Human-induced climate change is one of the greatest threats to humanity in the 21^{st} century. National Oceanic and Atmospheric Administration (NOAA) defines climate change as any changes in the Earth's climate due to natural variability or human activity [1]. Since 1880, the global average temperature has increased by 1.42°C over land surface and by 0.69°C over ocean surfaces that is free of ice at all times as shown in Figure 1.1B. Human activities such as burning fossil fuels, deforestation and soil disturbance have increased the carbon dioxide, methane, nitrous oxide, halocarbons, and other gas concentrations in the atmosphere which are the main contributors to the Earth's warming [2].

Climate change has detrimental effects on biodiversity. The effects include extreme weather, decreasing in ice masses, rising of sea level, and irregular reproduction and migration patterns in animal and plant species [3].Since 1980, the global mean CO_2 level continues to increase (Figure 1.2) due to fossil fuels and is projected to exceed 900 ppm by the end of the century [4]. Unfortunately,

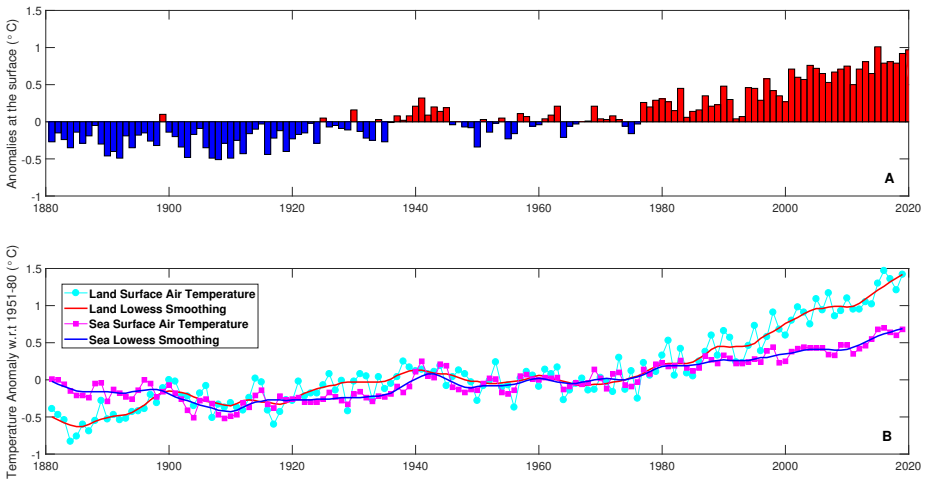

FIGURE 1.1: **(A)** The change in global average temperature over land and ocean surfaces from 1880 to November 2020 w.r.t the 20^{th} century average; warming since the 1970s is attributed to the increasing in greenhouse gases' concentration [2]. (**B**) Global average temperature anomalies of land and ocean surfaces is shown separately (Data obtained from NOAA).

fossil fuels (coal, oil and natural gas) are still the primary energy sources worldwide, and in 2018, it accounted for about 64 percent of the world energy consumption (Figure 1.3). As the world population increases, the energy demand increases with fossil fuels being the primary sources [5] [6]. The Kaya identity can be used to estimate the total CO_2 emissions from human sources:

$$C = \frac{C}{E} \cdot \frac{E}{GDP} \cdot \frac{GDP}{P} \cdot P \tag{1.1}$$

where C, E, $\frac{C}{E}$, $\frac{E}{GDP}$, $\frac{GDP}{P}$ and P are CO_2 emissions, energy consumption, emission coefficient effect, energy intensity, affluence (standard of living), and world's

population, respectively [7]. Global population growth rate is projected to decrease by the year 2050 [8]. From Equation 1.1, reducing carbon footprint is the most effective and realistic way in decreasing the overall CO_2 emissions. Environmental problems aside, fossil fuels are finite resources that are predicted to be depleted within the century based on the Hubbert curve[9].

1.2 Clean and Renewable Energy Sources For Addressing Climate Change

The three important criteria when it comes to clean energy are high power capacity to support global demand, sustainability, and cost effectiveness. In terms of power capacity, the projected annual global power consumption in 2050 is 30 TW [10]. Abbott made a comparasion between different renewable and nuclear energy sources for the three criteria with the assumption that all sources have the highest efficiencies [9]. To summarize the results, out of all the currently available renewable sources, only solar power is able to meet the projected global demand (Table 1.1). Additionally, on average 166 PW of solar power hits the Earth's surface [9].

This enormous solar power will help to account for efficiency problems of any solar devices we might encounter. In term of sustainability, the sun will remain at its current state for 5.4 billion more years before entering the red giant state where the Earth will already have become uninhabitable [11]. Nuclear power is also considered a clean power source and has the capacity to meet the global demands, but it is not in the scope of this thesis.

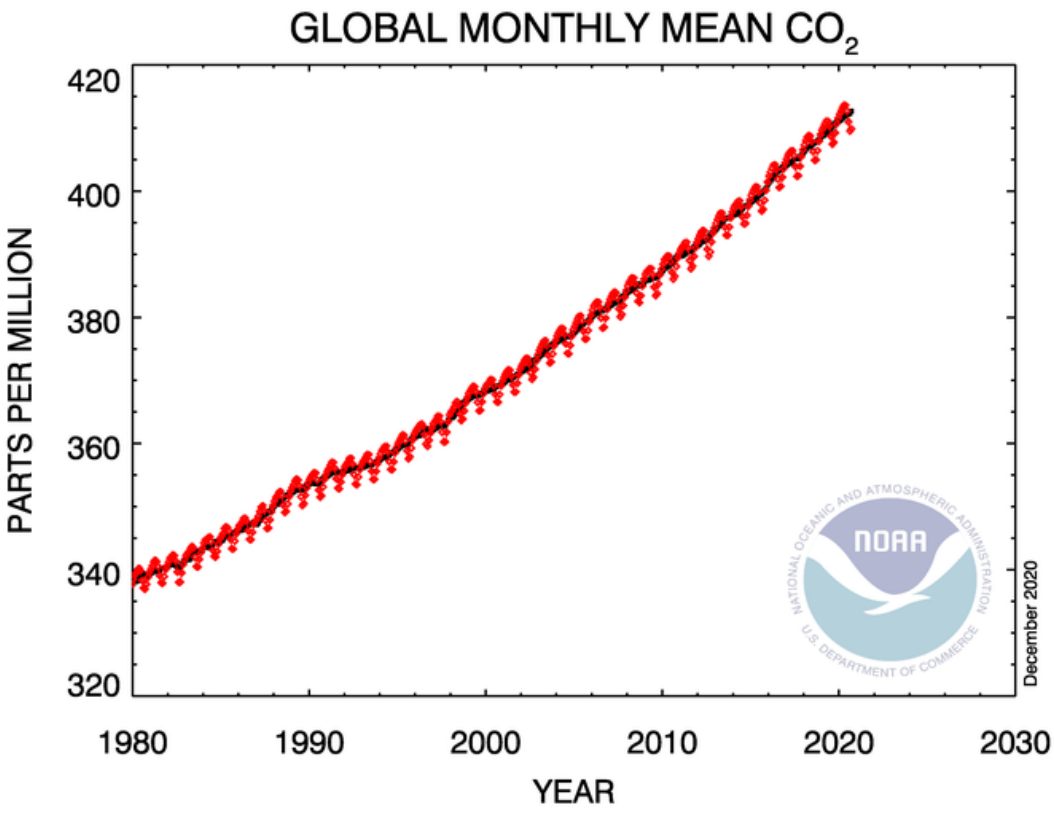

FIGURE 1.2: The monthly average of global CO_2 concentration since 1980. The red and black lines represent the monthly mean values and the monthly mean values with correction for the average seasonal cycle, respectively. The data is expressed as the number of molecules of CO_2 divided by the number of all molecules in air, including CO_2 and excluding water vapor. More details on the methods can be found on www.esrl.NOAA.gov under NOAA/GML calculation of global means. Figure courtesy of NOAA.

1.3 Solar Energy Storage Methods

One major disadvantage of solar energy is intermittency due to the fluctuation with the time of the day and the weather. Hence, the energy must be collected

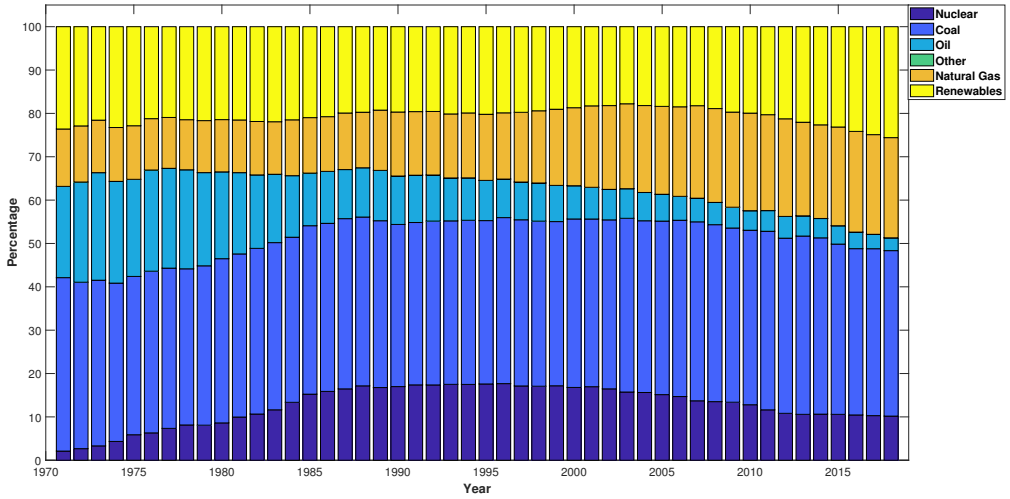

FIGURE 1.3: World electricity generation mix by fuel (1971-2018). The data doesn't include other forms of energy such as thermal energy. On average, 67% of the world's electricity was from fossil sources and only 21% was from renewable sources. Data courtesy of IEA.

Energy source	Max. power (TW)	% of Total Solar
Total surface solar	85,000	100%
Desert solar	7650	9%
Ocean thermal	100	0.12%
Wind	72	0.08%
Geothermal	44	0.05%
River hydroelectric	7	0.008%
Biomass	7	0.008%
Open ocean wave	7	0.008%
Tidal wave	4	0.003%
Coastal wave	3	0.003%

TABLE 1.1: An estimate of power outputs of different renewable sources assuming 100% efficiency [9]. Only solar energy has the capacity to meet the global demand.

and stored during peak times. There are two main forms of solar energy: electrical energy from photovoltaic panels and thermal energy from concentrated solar power [12]. Table 1.2 gives a summary of the different storing methods.

Electrical energy storage		
electrical energy storage	mechanical energy storage	chemical energy storage
capacitors or superconducting magnetic devices.	flywheel, pumped hydroelectric, compressed air.	batteries, fuel cells, and flow batteries.
Thermal energy storage		
thermal energy storage	sorption storage	chemical energy storage
Sensible heat: changing temperatures of materials Latent heat: changing phases of materials.	chemical separations	solar hydrogen, solar metal and solar chemical heat pipe.

TABLE 1.2: Classification of solar energy storage methods[12]. Solar energy can be collected and stored during peak hours. Hou et al., 2011 discussed the implementations of these methods in details.

In short, solar energy can be directly transformed into heat by focusing sunlight or into electricity using photovoltaic cells [12]. The heat can be used to change the temperatures or phases of materials, or drive unfavorable chemical reactions as a mean of storing the collected solar energy. The collected electricity can be stored in electromagnetic or mechanical devices, or used to drive chemical reactions. In terms of energy density, only fuel cells are compatible to fossil fuels (Figure 1.4), making them one of the best candidates for clean energy converters.

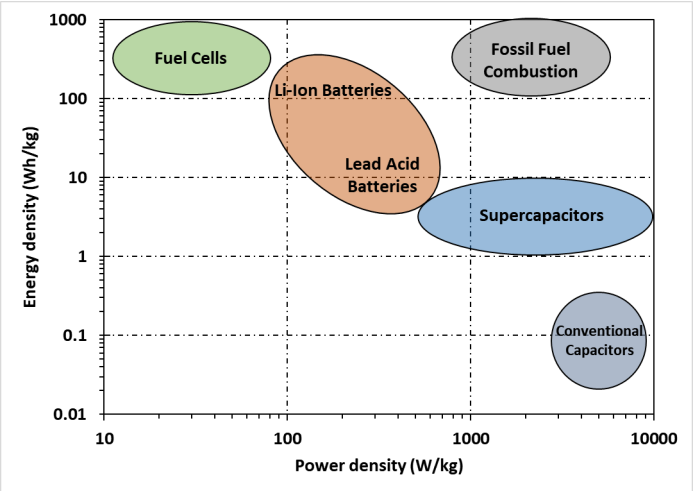

FIGURE 1.4: An overview of energy and power densities of different energy storage devices. Fuel cells have the highest energy density making them ideal as energy converters. Figure was adapted from [13].

1.4 Scope of thesis

Currently, wind and solar are the main sources of green energy, however, these are intermittent sources. A reliable, on-demand energy source is a fuel cell, which can also be portable. At this time, the most common fuels cells are based on use of hydrogen as the fuel and Pt as the catalyst. These fuel cells are not cost effective as they required platinum (Pt) as the catalyst. Additionally, implementation of the fuel cells is still a challenge due to their complexity; this in turn affects the energy efficiencies and life-times of the fuel cells. The goal of this study is to implement and characterize catalysts for single compartment membraneless fuel cell (SCMFC) with hydrogen peroxide (H_2O_2) as the clean energy carrier. Starting with Chapter 2, an overview of hydrogen fuel cells is given with

an introduction to H_2O_2 as an energy carrier, and how H_2O_2 is incorporated in SCMFC. Chapter 3 provides an overview of electrochemical techniques used to characterize the fuel cells. In Chapter 4, catalytic materials are introduced as well as a discussion of results for the fuel cells. Lastly, Chapter 5 provides a summary of the thesis and the future plans for the project.

Chapter 2

Fuel Cells

2.1 Reviews on Hydrogen Fuel Cells

As mentioned in Chapter 1, CO_2 level produced by fossil fuels can be significantly reduced or completely eliminated using hydrogen fuel cells. Figure 2.1 shows an example of a proton-exchange membrane hydrogen fuel cell. Detailed explanations of hydrogen fuel cell's operation can be found from [14][15]. In short, a hydrogen fuel cell consisted of two compartments which are separated by an electrolyte or a membrane. During operation, a source of hydrogen is supplied to the anode compartment. The cell's catalyst oxidizes the hydrogen to produce electrons and hydrogen ions (H^+). The H^+ ions pass through the electrolyte/membrane to the cathode compartment. On the other hand, the electrons can only travel to the cathode compartment via the provided conductive path. This produces a flow of electrons (current) that can be used as electricity. Once the H^+ ions and the electrons get to the cathode compartment, they will combine with the supplied oxygen/air to produce water.

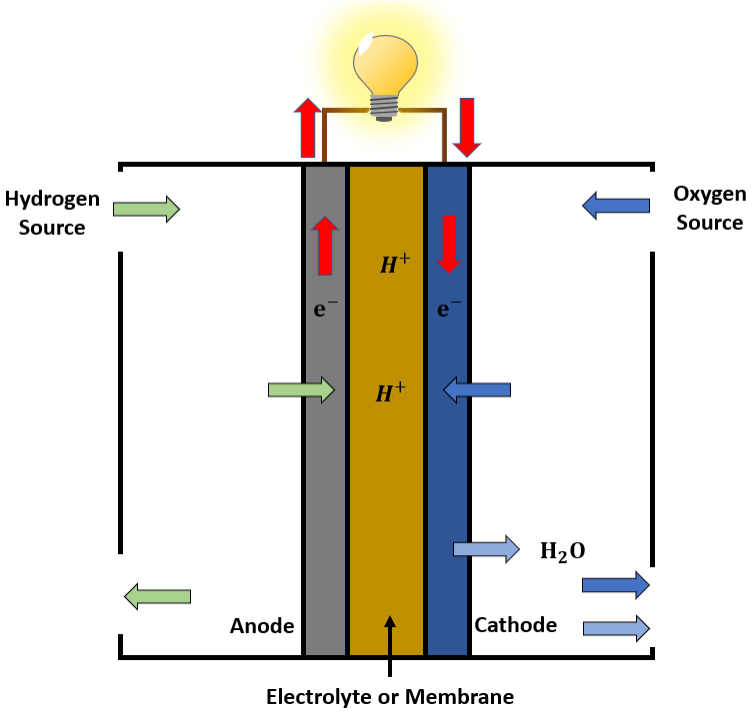

FIGURE 2.1: An example of proton-exchange membrane hydrogen fuel cell [15]. There exist different types of hydrogen fuel cells, however, the underlying physics is the same.

The redox reaction for hydrogen fuel cells, except for solid-oxide fuel cell (SOFC in Table 2.1), is as follow:

$$\text{Anode} : H_2 \rightarrow 2H^+ + 2e^- \qquad 0 \text{ V vs. NHE} \tag{2.1}$$

$$\text{Cathode} : \frac{1}{2}O_2 + 2H^+ + 2e^- \rightarrow H_2O \qquad 1.23 \text{ V vs. NHE} \tag{2.2}$$

$$\text{Total: } H_2 + \frac{1}{2}O_2 \rightarrow H_2O \qquad 1.23 \text{ V} \tag{2.3}$$

Hydrogen fuel cell comes in many flavors. Table 2.1 shows the five major main types of fuel cells and their applications. The name of a fuel cell type

reflects the type of electrolyte/membrane that is being used. One major disadvantage of hydrogen fuel cells is the cost of the catalytic materials. To date, platinum, oxides of ruthenium and iridium are the most competent catalysts for hydrogen fuel cells [16][17]. These materials are scarce and expensive which this does not fit the three criteria for clean renewable energy mentioned in Section 1.2.

FUEL CELL TYPE	COMMON ELECTROLYTE	OPERATING TEMPERATURE	TYPICAL STACK SIZE	ELECTRICAL EFFICIENCY	APPLICATIONS	ADVANTAGES	DISADVANTAGES
Polymer electrolyte membrane (PEM)	Perfluorosulfonic acid	<120°C	<1-100 kW	40% reformed 60% direct H_2	Backup power Portable power Distributed generation Transportation Specialty vehicles	Solid electrolyte reduces corrosion and electrolyte management problems Low temperature Quick startup and load following	Expensive catalysts Sensitive to fuel impurities
Alkaline (AFC)	Aqueous potassium hydroxide soaked in a porous matrix, or alkaline polymer membrane	<100°C	1-100 kW	60%	Military Space Backup Power Transportation	Wider range of stable materials allows lower cost components Low temperature Quick startup	Sensitive to CO_2 in fuel and air Electrolyte management (aqueous) Electrolyte conductivity (polymer)
Phosphoric acid (PAFC)	Phosphoric acid soaked in a porous matrix or imbibed in a polymer membrane	150-200°C	5-400 kW (liquid PAFC) <10 kW (polymer membrane)	40%	Distributed generation	Suitable for CHP Increased tolerance to fuel impuritites	Expensive catalysts Long startup time Sulfur sensitivity
Molten carbonate (MCFC)	Molten lithium, sodium, and/or potassium carbonates, soaked in a porous matrix	600°- 700°C	300 kW- 3 MW	50%	Electric utility Distributed generation	High efficiency Fuel flexibility Suitable for CHP Hybrid/gas turbine cycle	High temperature corrosion and breakdown of cell components Long startup time Low power density
Solid oxide (SOFC)	Yttria stabilized zirconia	500°-1,000°C	1 kW - 2 MW	60%	Auxiliary power Electric utility Distributed generation	High efficiency Fuel flexibility Solid electrolyte Suitable for CHP Hybrid/gas turbine cycle	High temperature corrosion and breakdown of cell components Long startup time Limited number of shutdowns

TABLE 2.1: A comparison of the major main types of hydrogen fuel cells. The table was duplicated from the Office of Energy Efficiency & Renewable Energy [18].

2.2 Single Compartment Membraneless Hydrogen Peroxide Fuel Cell

Recently, hydrogen peroxide (H_2O_2) has been considered as a clean energy carrier that can be used as both fuel and oxidant in fuel cell technologies [19] [20] [21]. At 100% efficiency, H_2O_2 can decompose into water and oxygen, outputting 117 kJ/mol [21]. Furthermore, H_2O_2 can be produced from seawater or water and oxygen in acidic environments using solar energy [22][23] [24] making it an ideal candidate for fuel cell technologies. With an appropriate material selection, the oxidation and reduction of H_2O_2 at the cathode and anode are [23]:

$$\text{Anode} : H_2O_2 \rightarrow O_2 + 2H^+ + 2e^- \qquad 0.68\text{V vs. NHE} \tag{2.4}$$

$$\text{Cathode} : H_2O_2 + 2H^+ + 2e^- \rightarrow 2H_2O \qquad 1.77 \text{ vs. NHE} \tag{2.5}$$

$$\text{Total: } 2H_2O_2 \rightarrow O_2 + 2H_2O \qquad 1.09 \text{ V} \tag{2.6}$$

Figure 2.2 shows the schematic of a single compartment membraneless H_2O_2 fuel cell (SCMHFC). Both the cathode and anode are immersed in an acidic solution of H_2O_2.

The theoretical output potential of the reactions is 1.09V vs. NHE which is lower but comparable to hydrogen fuel cells (1.23 V) and direct MeOH fuel cell (1.21 V) [23]. However, the simple SCMHFC structure has an advantage that it does not require membranes to separate the cathode and the anode as in the case of hydrogen fuel cells. Furthermore, the results presented in Chapter 4 have shown that catalytic materials for H_2O_2 can be inexpensive and cost effective at large scale. Using renewable fuel source with clean byproduct and low

implementation cost, SCMHFC is a promising device to combat climate change.

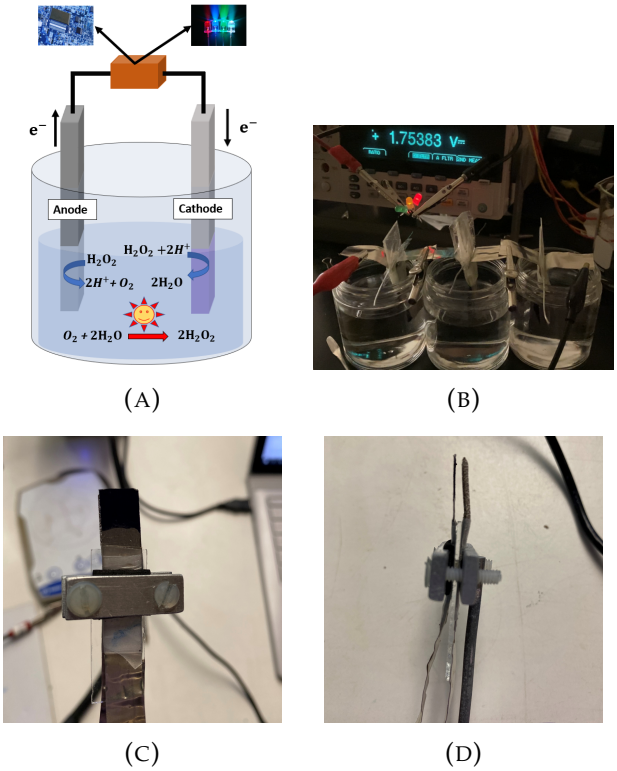

FIGURE 2.2: (A) SCMH fuel cell setup with both the cathode and anode are an acidic solution of H_2O_2. H_2O_2 can be produced from water and oxygen. (B) A photo of a three stack SCMH fuel cell to increase the cell's voltage. At the maximum theoretical value, the potential is still very low for practical usages. (C) and (D) A simply electrode setup with a glass slide separating the anode and the cathode.

Chapter 3

Electrochemical Methods for Fuel Cell Characterization

3.1 Introduction To Fuel Cell Reaction Kinetics

In electrochemical reactions, electrons are transferred between an electrode and a chemical species at the interface between an electrode and an electrolyte [15][25][26]. The direction of electron flow depends on the potential of the electrode relative to the electrolyte as shown in Figure 3.1 [15][25][26]. By changing the potential of the electrode in an electrode-electrolyte system, the current density j, defined as current per unit area (A/cm^2), can be measured. The reaction kinetics of a system can be understood by examining the current density response.

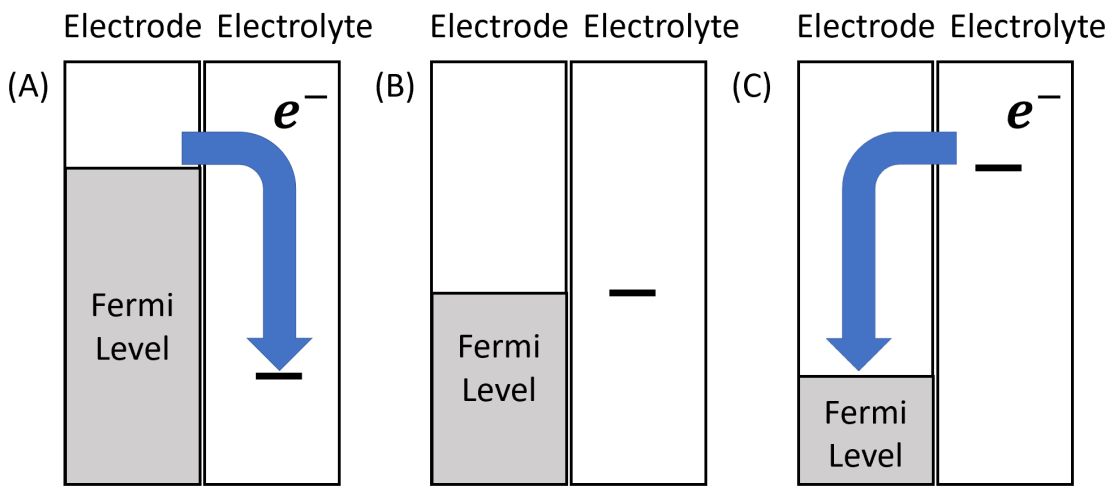

FIGURE 3.1: The potential of the electrode, i.e. the Fermi energy level of the electrons, is (A) higher than the electrolyte (B) equal to the electrolyte (C) lower the electrolyte. The electrons transfer from high to low potential. Figures adapted from [15][26].

In order for a chemical species to undergo a reaction, they must first overcome the activation barrier (Figure 3.2). The activation energy is the energy required for the chemical species to overcome the barrier. It directly affects the reaction rates which in turn affects the current density of the electrochemical system. The relationship can be described as the following:

$$J = c_R^* f e^{\frac{-\Delta G^\ddagger}{RT}}, \tag{3.1}$$

$$j = nFJ \tag{3.2}$$

$$j = nFc_R^* f e^{\frac{-\Delta G^\ddagger}{RT}} \tag{3.3}$$

where J is the reaction rate, c_R^* is the reactant surface concentration (mol/cm^2), f is the decay rate to products, R is the gas constant, T is the temperature, n is the number of electrons and F is the Faraday's constant.

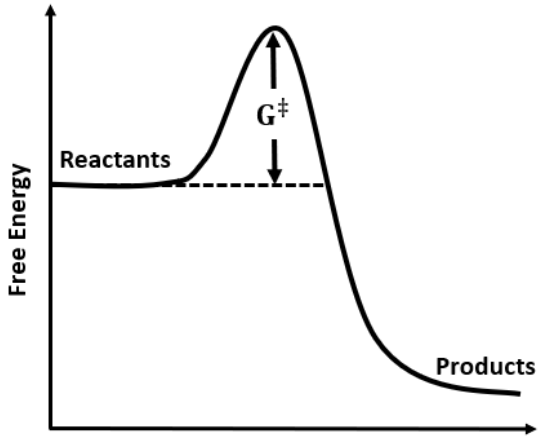

FIGURE 3.2: The energy diagram for a chemical reaction. The reactant species must overcome the potential barrier, $G^{\ddagger}$, for the reaction to occur. Additionally, there is a non-zero probability the electrons will fall back to the reactant side at the peak. Catalysts and external energy can be used to lower the barrier and modify its shape [15]. Figures adapted from [15].

Equation 3.3 provides several options to improve the current density. Increasing the reactant concentration, temperature of the fuel cell and active sites can increase the current density[15]. Similarly, decreasing the activation barrier by choosing the appropriate catalysts will also increasing the current density. For this thesis, only the catalytic materials and the surface structures were examined while keeping the other parameters fixed.

3.2 Cyclic Voltammetry

Cyclic voltammetry is a powerful electrodechemical technique, commonly used to study oxidation and reduction of chemical processes. It is a half-cell technique as only one electrode of a fuel cell is studied at a time. The standard technique involves a set of three electrodes: a working electrode, reference electrode and counter electrode [15][25][26]. A potentiostat is used to vary the potential between the working and reference electrodes while measuring the current between the working and reference electrodes as shown in Figure 3.3a. Recall in Section 3.1, the current density in an electrode chemical system is determined by the potential of the electrode relative to the electrolyte. By varying the potential of the electrode as shown in Figure 3.3b, the reduction or oxidation current density of the system can be measured. The potential values at which the reduction and oxidation currents begin to flow are defined as the onset potentials of reduction or oxidation [25]. A reference electrode, whose potential remains constant regardless of the current flow, is used to accurately measure the potential[25][26]. For fuel cell studies, the working electrode is the cathode or anode.

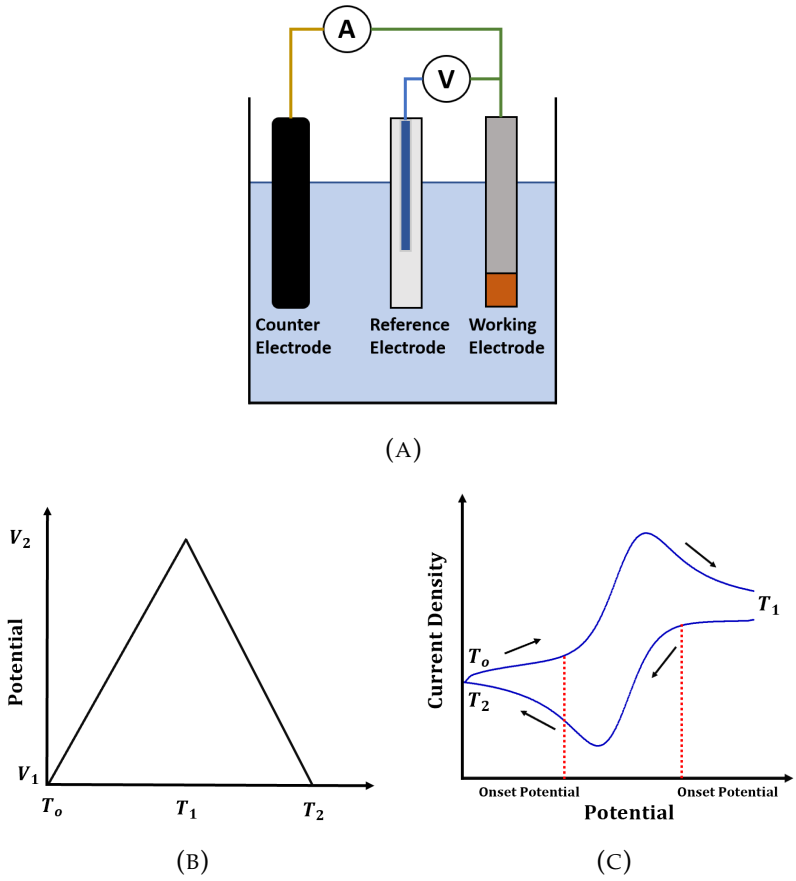

FIGURE 3.3: (A) Potentiostat setup to study half cell. (B) Voltage profile between the working and the reference electrodes. (C) The current response of the half cell as a function of the sweeping potential.

The choice of reference and counter electrodes depends on the system in study [25] [26]. For example, the surface area of the counter electrode must be greater than the surface area of the working electrode so that it does not inhibit the reactions that occurs at the working electrode [26]. The sweep rate of the potential also affects the observed current [25][26]. This can be seen from the

Randle-Ševčík equation

$$j_p = 0.446nFAC^0(\frac{nF\nu D_o}{RT})^{1/2} \tag{3.4}$$

where j_p is the observed current density, n is the number of electrons involved in the reaction, A (cm^2) is the geometric surface of the electrode, D_o (cm^2s^{-1}) is the diffusion coefficient of the oxidized analyte, and C^o (mol cm^{-3}) is the bulk concentration of the analyte. Faster sweep rates decrease the size of the diffusion layer which increases the current densities [26]. The cyclic voltammetry measurements in this study were done using an Ag/AgCl reference electrode and 1.0 cm diameter carbon rods as the counter electrodes in 0.1M HCl with and without 0.5M H_2O_2 at 10 mV/s to determine the onset potentials of the catalysts. The onset potentials are used for anode selections.

3.3 Linear Sweep Voltammetry

Similar to cyclic voltammetry technique, linear sweep voltammetry (LSV) technique involves changing the potential or current density between the working and reference electrodes. However, the potential only sweeps in one direction in LSV. Additionally, LSV is commonly used to study a full cell in which the reference electrode also acts as the counter electrode [15]. In literature, LS voltammograms, also called polarization curves are the standard way of reporting the overall performance of the fuel cell[15]. In an ideal fuel cell, the voltage remains constant as the current density changes. However, in a real cell, there are three loss modes associated with the current density (Figure 3.4): activation

loss, ohmic loss and concentration loss [15][25]. The operating voltage of a fuel cell with the losses is:

$$V = E_{thermo} - (\Sigma_{i=1}^{i=2}(a_i + b_i \ln(j)) + jR_{ohmic} + c \cdot \ln\frac{j_L}{j_L - j}) \tag{3.5}$$

where E_{thermo} is the predicted voltage of the fuel cell, a_i and b_i are empirical constants, j is the current density, j_L is the current limiting density, and R_{ohmic} is the total resistance of the electrolyte and the conducting components [15]. These losses in turn affect the output power density or performance of the fuel cell. The power density of a fuel cell can be found by multiplying the potential value and the corresponding current density on the polarization curve. In general, high performance fuel cell will produce high voltage, i.e. lower loss, at a given current density [15]. In this study, polarization method was extensively used to compare the performances of the catalysts.

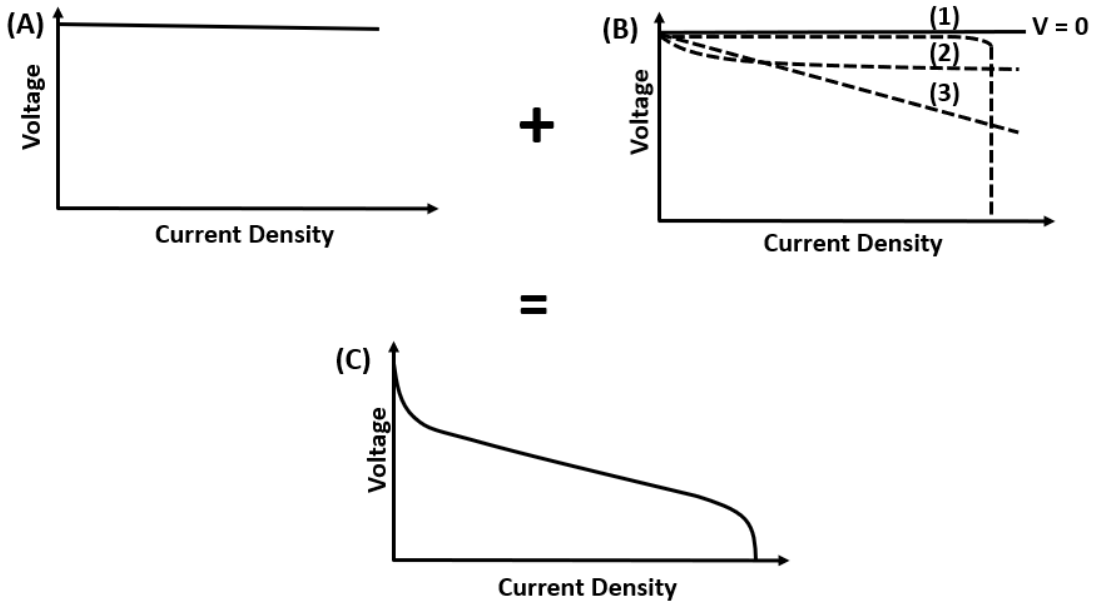

FIGURE 3.4: (A) A typical j-V curve of a battery or a power supply. The voltage remains constant for different load values.(B) Activation loss (B1), resistive loss (B2), and concentration loss (B3) in fuel cells. (C) An j-V curve of a fuel cell. Figures adapted from [15].

3.4 Electrochemical Impedance Spectroscopy

Fuel cells can be modeled as electrical circuits consisting of resistors, capacitors and inductors (Figure 3.5a) [15]. The impedance of a fuel cell, which relates to the losses, can be determined by examining the frequency response of the cell. Electrochemical impedance spectroscopy (EIS) involves perturbing a cell with a sinusoidal wave with an rms amplitude of approximately 10 mV at different frequencies and measuring the current density response. The impedance for the electrical components are:

$$X_R = R \tag{3.6}$$

$$X_C = \frac{1}{\omega C} \tag{3.7}$$

$$X_L = \omega L \tag{3.8}$$

with R, C and L being the resistance, capacitance and inductance of the components, respectively, and $\omega(\text{rad/sec})$ is the radial frequency of the sinusoidal wave. Equation 3.7 and 3.8 show that the impedance increases or decreases at different frequency. This can be utilized to study the losses of a fuel cell in detail. The results are represented on a complex impedance plane as shown in Figure 3.5b. Different softwares can be used to fit and estimate the impedance of the electrical components. The resistive elements represent the activation losses of the electrodes and the resistances of the electrodes, electrolytes and wires [15][27]. The capacitance can be associated with the porosity of the electrodes [15][27]. A diffusion element called Warburg impedance (labeled W in Figure 3.5) represents partial or complete mass transport diffusion control [27]. Warburg impedance is more prominent at the lower frequency and can be identified by a 45^o line on the Nyquist plot [15][27]. The rms voltage of the waveform should be closed to the value where mass transport loss is dominant. While providing a powerful tool to characterize fuel cell systems, EIS results can be difficult to interpret, and hence, was used qualitatively in this study. Gamry Instruments software was used to perform fittings. Each model fitting came with a goodness of fit value and percentage errors for the impedance. The models that had the lowest goodness of fit value and percentage errors were chosen to represent the systems. Also, Gamry Instruments software provided a tool to calculated the capacitance from the fittings. More information in the methods

used can be found in Gamry Instruments' application note [28].

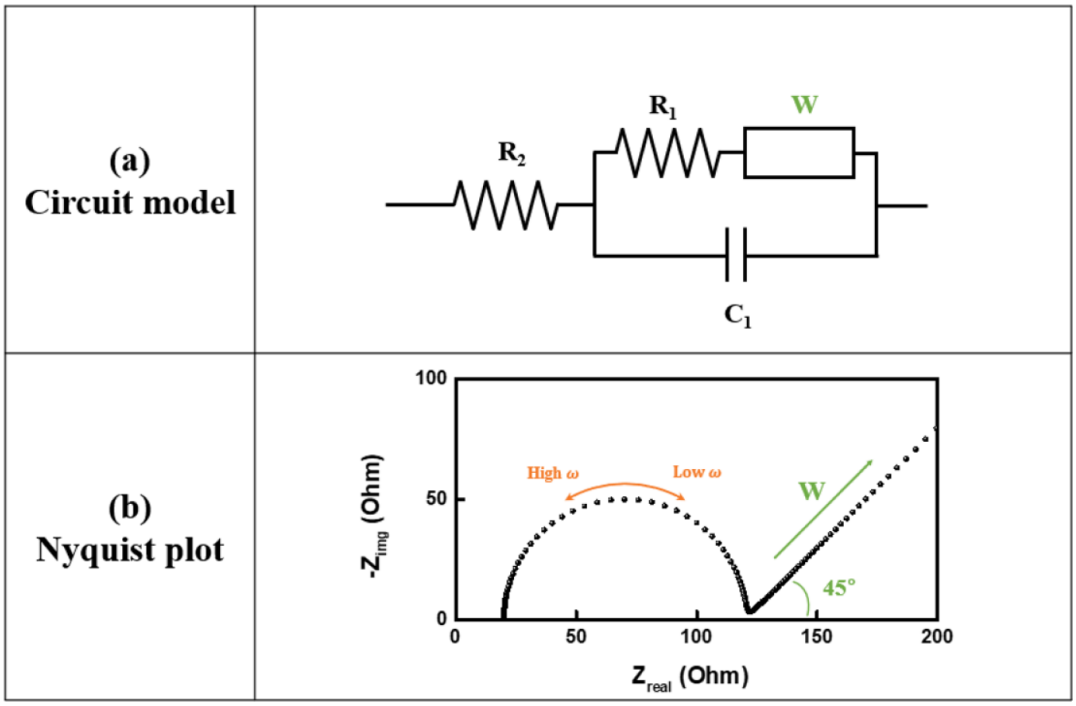

FIGURE 3.5: (a) The circuit equivalent for a single electrode/electrolyte interface where R_1 is resistance of the electrode, R_2 is the resistances of the electrolyte and the cables/connectors, C_1 is the capacitance of the double layer, and W is the linear diffusion element. (b) The Nyquist plot of EIS experiment. Figure courtesy of [27].

Chapter 4

Results and Discussion

4.1 Introduction

Several catalysts were examined in SCMFC with H_2O_2 acting as both fuel and oxidizer. The results of these studies are presented in this chapter. First, the cyclic voltammetry technique was used to determine the onset reduction potential of H_2O_2 on the cathode. The results were used for the anode selection process. For several materials, the onset reduction potentials were already known. Next, for comparative studies, the polarization technique was used to determine the open circuit potentials and the maximum output powers of the fuel cells. Lastly, the EIS technique was used to qualitatively determine losses of the fuel cells.

4.2 Metallophthalocyanine Electrocatalysts

4.2.1 Introduction

In nature, the most common enzymes found in plants and animals contain porphyrin complexes, which are responsible for catalytic aerobic oxidation, reduction, transport of dioxygen, as well as destruction of peroxides [29][30]. However, using synthetic porphyrin complexes (Por) as catalysts is not practical due to high cost of preparation at large scale [31]. Recently, metallophthalocyanine (MPcs), which are structurally similar to Por, has gained many attractions for their catalytic properties [30-33]. Figure 4.1 shows the structure of MPc and porphyrins. High oxidation and reduction properties have been observed by incorporating metal atoms into the PC ring forming a π-electron conjugation [30][32]. Furthermore, MPcs exhibit high chemical and thermal stability, which are ideal in fuel cells, and are readily accessible in a large scale at low cost [31].

The choice of transition metals were based on their catalytic properties. FePc have shown to be one of the most effective catalytic materials for ORRs where active sites locate at the FeN_4 moieties which has been attributed to the uncommon spin state of Fe(II) electron [34-37]. For this reason, Fe_xN(x=2,4) was also chosen as a catalyst to compare with FePc performance. Copper based complexes exist in many biological processes as catalysts for ORR [33][34]. Cobalt metal complexes have been shown to be exceptional H_2O_2 catalyst and have been used in H_2O_2 sensors [40-42]. Cobalt Pc has also been used as an effective catalyst in microbial fuel cells [43-46]. Hence, CuPc and CoPc were chosen as catalysts in this study. The results for this study have been published on ECS

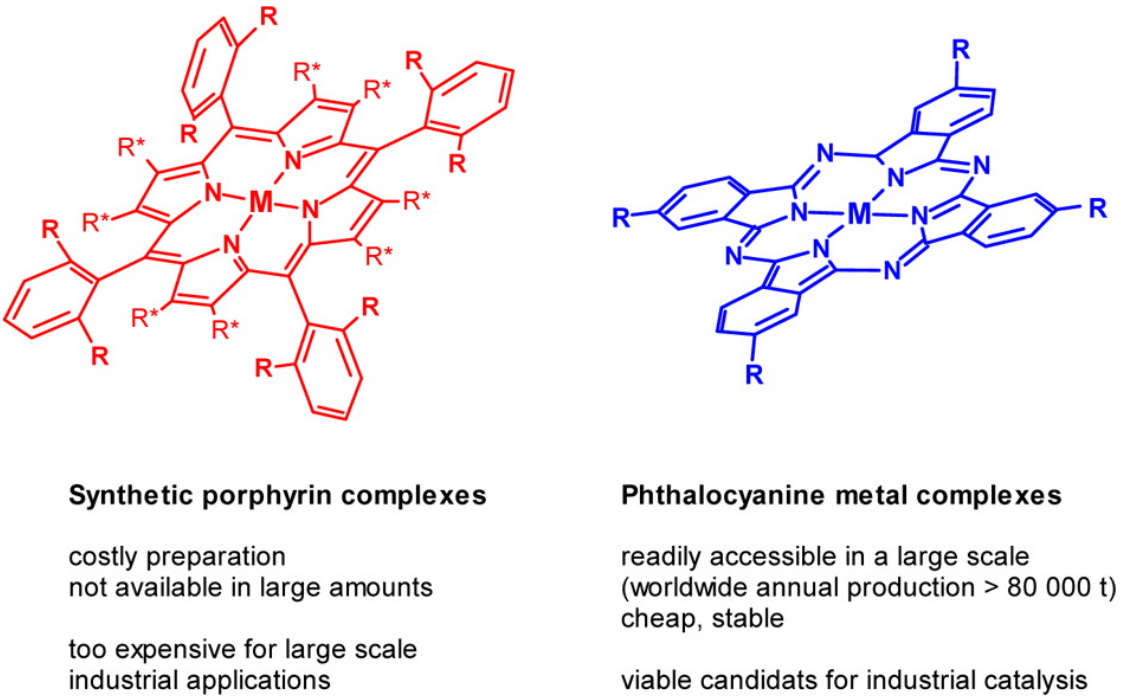

FIGURE 4.1: MPc structure vs. Porphyrin. Figure courtesy of [31].

Journal of Solid State Science and Technology.

4.2.2 Electrode Preparations

Fe(II)Pc (96%) and Co(II)Pc were purchased from Alfa Aesar, Cu(II)Pc β-form (97%) from Aldrich Sigma and Fe_xN from BTC Chemical. The electrocatalytic reduction of $H_2O_2$was examined in a three-electrode cell with a strip of carbon paper coated with MPc or Fe_xN as cathodes, a Ni mesh as the anode, and an Ag/AgCl reference electrode. The Ni anode and MPC cathode act as selective electrodes for the H_2O_2oxidation and reduction, respectively. Thus, a one-compartment fuel cell without a membrane separator between the anode and cathode can be realized. One of the drawbacks of PC complexes is their low

electron conductivity [30]. Hence, to improve the electrocatalytic activity, conductive materials were necessary in preparing the electrodes. For this purpose, the MPCs were mixed with carbon black, multi walled carbon nanotubes, and polyvinylidene difluoride (PVDF) as the binder. The ratios of the powder mixtures were 80% MPC powder, 9% MWCNTs, 9% PVDF binder, and 2% carbon black. N-Methyl-2-pyrrolidone (NMP) was added to the powder mixtures to produce a paste which was applied to carbon paper strips that had been rinsed with ethanol and dried in an oven at 60^{o}C for 15 minutes. The physical surface area of the applied region was 1 cm^2 The electrodes were left to dry overnight. Lastly, the electrodes were annealed at 110^{o}C under low vacuum and cooled overnight.

4.2.3 Results and Discussion

Cyclic voltammetry experiments were carried out with the electrodes immersed in an electrolyte that consisted of 40 mL equivolume of 0.5 M $H_2O_2$and 0.1 M HCl. Ag/AgCl served as the reference electrode (reported vs. SCE) and 1 cm diameter carbon rods were used as the counter electrodes for the experiments. A Gamry potentiostat was used for the electrocatalytic measurements. Before the experiments began, the cells were allowed to stabilize for 10 minutes. All experiments were done at 10 mV s^{-1} sweep rate. Each material was examined in electrolytes with and without H_2O_2 to determine the background effect. Cyclic voltammograms of the four catalysts examined are shown in Figure 4.2, where the voltage sweeps without $H_2O_2$are shown in orange and with H_2O_2 in blue. From the sweeps with H_2O_2, the potentials for onset of the catalytic currents of

the peroxide reduction were observed. The reduction onset potentials of FePC, CoPC, CuPC and $Fe_{x=2,4}N$ were 0.56 V, 0.42 V, 0.51 V and 0.57 V, respectively.

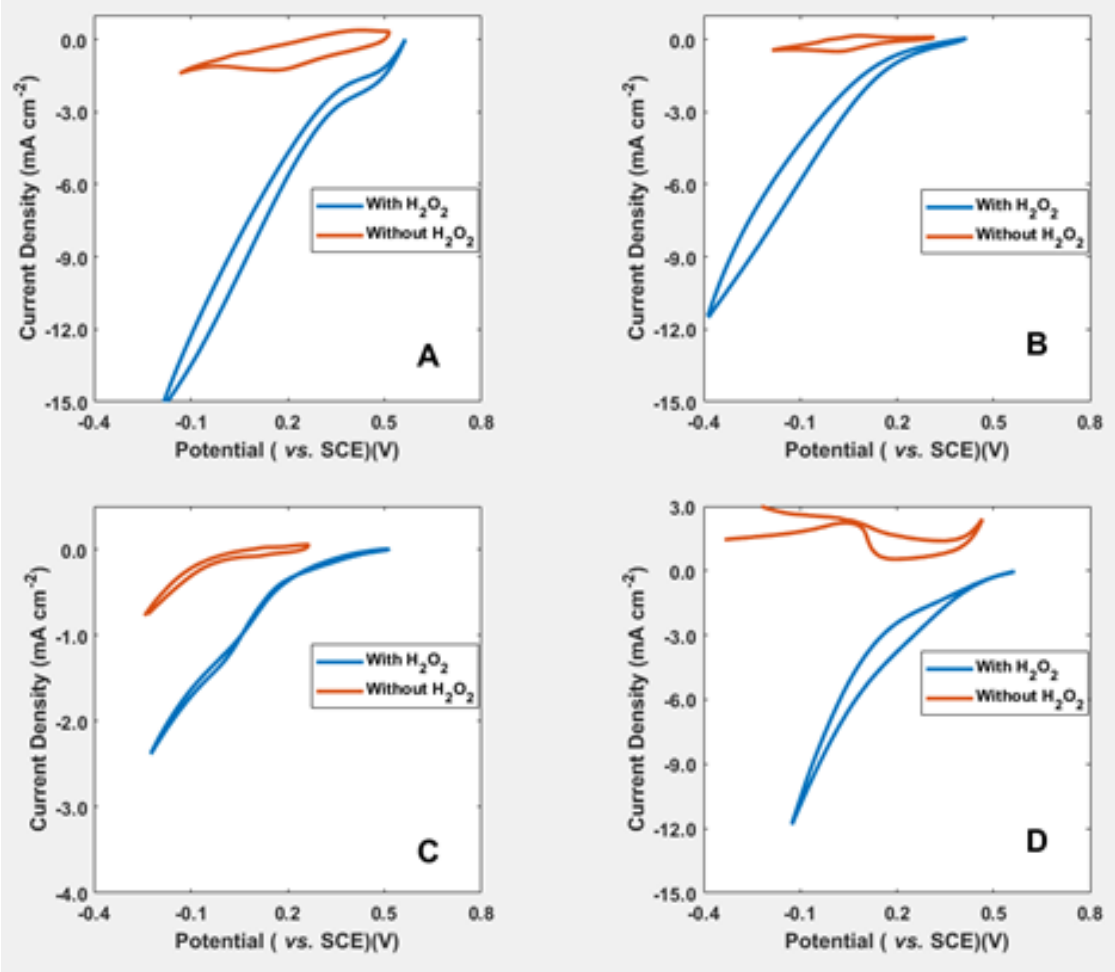

FIGURE 4.2: Cyclic voltammograms of H_2O_2 on carbon paper modified with supported MPc complexes and $Fe_{x=2,4}N$. (A) FePC, (B) CoPC, (C) CuPC and (D) FexN. The measurements were made in 0.1 M HCl with (in blue) and without 0.5 M H_2O_2 (orange). Scan rate of 10 mV s^{-1} was used for the experiments

The performances of the fuel cells were examined by recording polarization curves via linear potential sweep voltammetry to determine the potential–current density and power density characteristics. The sweep rate for the polarization curves was 500 μA$\cdot$ s^{-1} and the electrolyte composition was the same as for voltammetry. The results are shown in Fig. 2. The OCPs of the fuel cells were measured at the beginning of the polarization curves. The OCPs for FePC, CoPc, CuPc, and Fe$_{x=2,4}$N were determined to be 0.56 V, 0.48 V, 0.57 V, and 0.58 V, respectively. The power densities of the fuel cells were FePC and CoPC, CuPC, and Fe$_{x=2,4}$N were 2.8 mW$\cdot$cm^{-2}, 0.28 mW$\cdot$cm^{-2}, 0.27 mW$\cdot$cm^{-2} and 0.76 mW$\cdot$cm^{-2}, respectively.

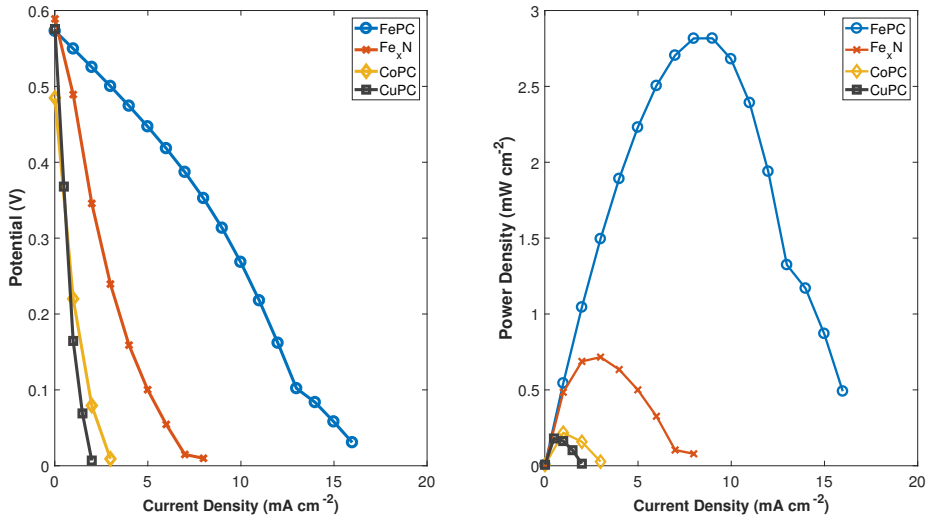

FIGURE 4.3: Polarization curves for MPcs and Fe$_{x=2,4}$N. While all open circuit potentials of the material, except CoPc, are similar, FePc has the highest maximum power density.

Electrodechemical impedance spectroscopy in the range of 1 mHz to 1 MHz

was used to better understand the behaviors of the fuel cells.The rms voltage of the waveform was chosen to be 10 mV where diffusion loss (Warburg impedance) would be dominant. The Nyquist plots of the experiments are shown in Figure 4.4 and a summary of the fit results is shown in Table 4.1. FePc fuel cell has the lowest impedance (26 Ω measured) and CuPc fuel cell has the highest impedance (6 kΩ measured) of the 4 fuel cells in study. From the fit results, FePc activation loss is magnitudes lower compared to the other fuel cells which might be the main factor for the output current density. In CuPc fuel cell, as the frequency approach 1 mHz, the system became unstable due to the unstable OCP. The effect can be seen in Figure 4.4c where the fit result and the measured result diverged. Warburg impedance did not appear within the frequency range for all four fuel cells. An attempt to extend the low frequency limit (data not shown) to measure the impedance. However, the systems became unstable as the anode was dissolving. Comparing the capacitances in Table 4.1, FePc exhibits high capacitance, at 2.35 $F \cdot cm^{-2}$, which suggested that FePc cathode has high porosity compared to the other three fuel cells. Low activation losses and highly porous structures might be the main factors for FePc fuel cell's high performance.

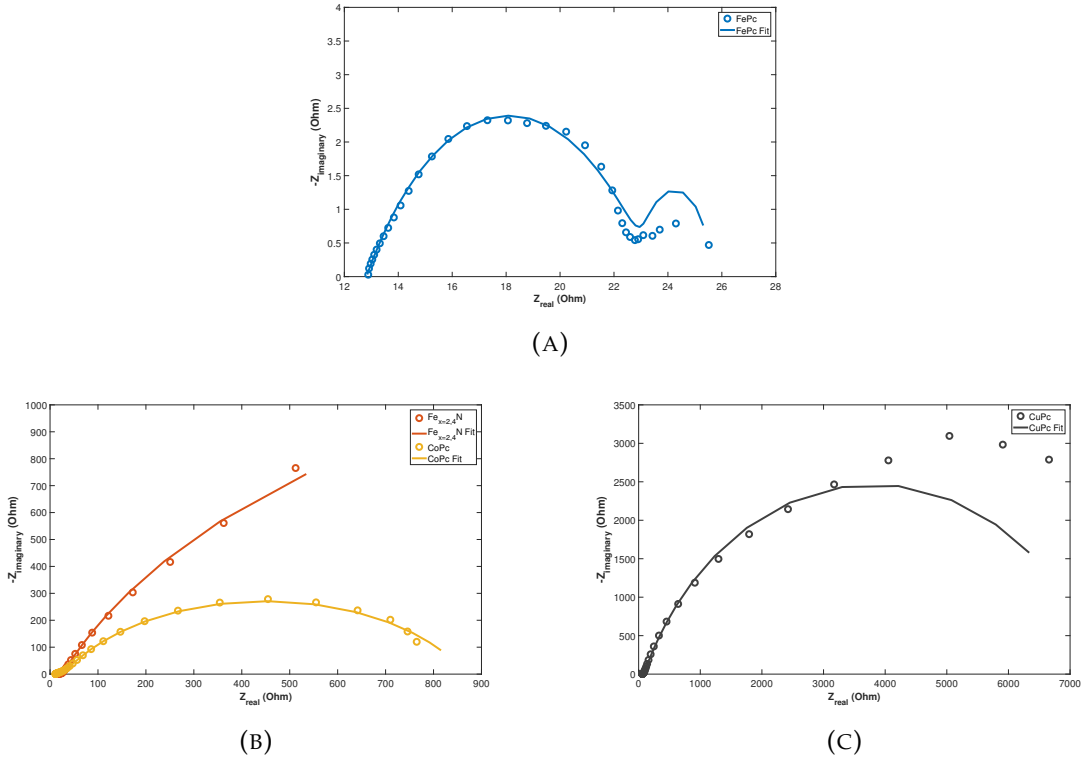

(A)

(B)

(C)

FIGURE 4.4: The Nyquist plots and fitting lines of MPc and $Fe_{x=2,4}$ fuel cell EIS experiments. The results are on different plots due to the range differences with (A) results for FePc, (B) results for CoPc and $Fe_{x=2,4}$ and (C) CuPc. FePc fuel cell impedance is magnitudes lower compared to the other three fuel cells. The results agreed well with the polarization results (Figure 4.3).

	Cathode Resistance (Ω)	Anode Resistance (Ω)	Total Resistance (Ω)	Cathode Capacitance (mF)	Anode Capacitance (μF)
FePc	2.25	10.54	12.8	2.35 x 10^3	367
$Fe_{x=2,4}N$	3.19 x 10^3	7.912	3.22 x 10^3	33.2	192
CoPc	791.6	27.39	830	1.80	126
CuPc	7.72 x 10^3	30	7.79 x 10^3	2.97	0.109

TABLE 4.1: A summary of EIS fitting results for MPc and $Fe_{x=2,4}N$ experiments. Different equivalent circuit models were used for the fittings. Models with the lowest goodness fit values and error values for the components were reported. Gamry software parallel resistance was used to calculated the capacitances.

4.3 Vitamin B12

4.3.1 Introduction

As mentioned in Section 4.1, cobalt metal complexes are promising catalytic materials for H_2O_2. Cobalamin/Vitamin B12 has been projected as one of the most competent electrocatalyst for H_2O_2 sensing [35]. Figure 4.5 shows the structure of Vitamin B12. Recently, cobalamin/Vitamin B12 functionalized N-doped graphene was used for H_2O_2 sensing [17]. Bhat et al. showed that the material was electrochemically stable and reusable electrocatalyst. Hence, a short experiment was done with Vitamin B12 as a cathode material for SCMHFC. It was noted that unmodified cobalamin could be unstable under acidic environment [17]. Hence, two different electrode preparation methods were used for a comparative study.

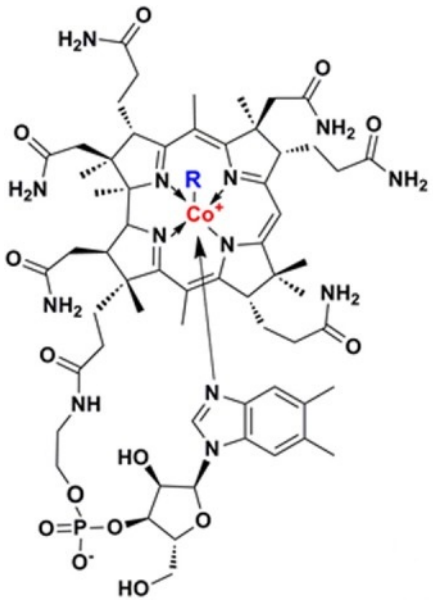

FIGURE 4.5: Molecular structure of Cobalamin/Vitamin B12. Image Courtesy of [36].

4.3.2 Electrode Preparations

The Vitamin B12 powder was purchased from BTC Chemical. Two different electrode preparation methods were used to make Vitamin B12 electrodes. The first method was similar to the method used in 4.1 for metallophthalocyanine, denoted as the paste method. For the second method, denoted as the ink method, a mixture consisted of Vitamin B12 (54.9 mg), MWCNTs (3.2 mg), carbon black (3.5 mg), isopropanol (10 mL), and DI water (2 mL) was added to a closed glass container and sonicated for 20 minutes. An additional 5% wt Nafion (0.30 mL) was added to the mixture and further sonicated for 20 minutes. Next, the mixture was transferred to a mist sprayer and sprayed on a carbon paper strip under a fume hood. A lamp was used to accelerate the drying process. Lastly, The

electrode was annealed under vacuum at 60^{o}C for two hours and left to cool overnight. The total weight added to the carbon paper strip was 24.1 mg.

4.3.3 Results and Discussions

The cyclic voltammetry and EIS data are not available for the experiments. The polarizing experiments were carried out in equivolume of 0.5 M $H_2O_2$and 0.1 M HCl at 1 μA $\cdot$cm^{-2} scan rate. The results are shown in Figure 4.6. The OCPs for the ink and paste methods were 0.49 V and 0.48 V, respectively. The output power densities of the ink-method and paste-method fuel cells were 0.065 mW$\cdot$cm^{-2} and 0.18 mW$\cdot$cm^{-2}, respectively. The low output power densities was likely due to the poor contact between the ink and the carbon paper strip and not enough catalyst mass. A problem arose during the experiments. The cathode materials began to dissolve immediately after submerged in the analytes. An example of the incident is shown in Figure 4.7.

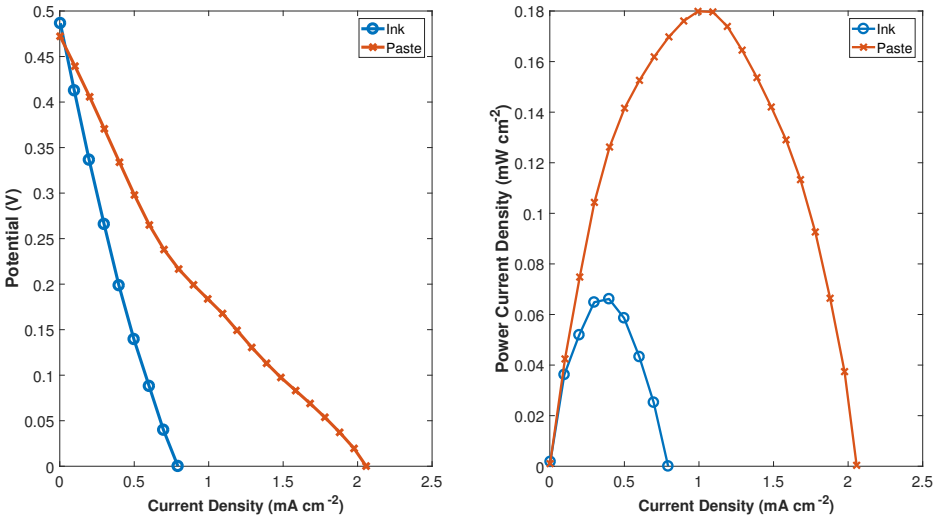

FIGURE 4.6: Polarization curves for Vitamin B12. Two different electrode preparation methods were used to create the electrodes.

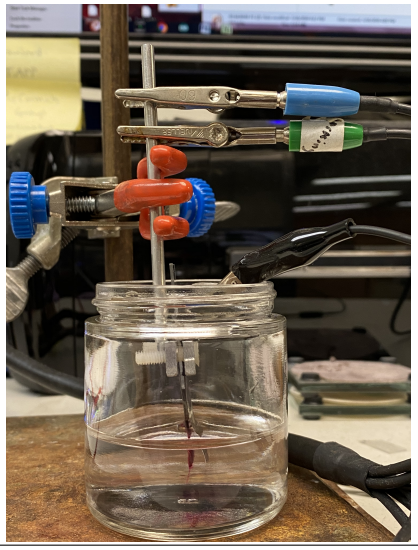

FIGURE 4.7: Electrode bleeding effect of Vitamin B12 electrodes immediately after submerged in the analytes.

4.4 Prussian Blue

4.4.1 Introduction

Prussian blue, iron(III) hexacyanoferrate(II) or ferric ferrocyanide was found in 1706 [37]. Kraft provided a summary of prussian blue history and its applications [37]. Prussian blue is a mixed valence transition metal complex compound that possesses a cubic lattice structure Fe(III)-C-N-Fe(II)-N-C sequences. Since its discovery, prussian blue has been widely used in many different applications such as poison antidote for radioactive cesium and thallium in human body [38] [39], electrochroism [40] and batteries [41]. Application of prussian blue has also extended to catalyst in fuel cells, microbial cells and microbial batteries. prussian blue has been used in glucose sensors to catalyze the reduction of prussian blue into water and oxygen [42][43]. Yamada et al. and Shaegh et al. have used prussian blue and its analogous as cathode materials in SCMH fuel cell. In this study, prussian blue's surface structure and composition were modified to examine the electrocatalytic activities of the cathodes in SCMFC. Porous Fe/Fe_3C nanoparticles, derived from prussian blue, exhibit high electrocatalytic activity compared to the unaltered prussian blue and has been used as anode material in supercapacitor [44]. Prussian blue and prussian blue analogous porous cube have also been used to boost its electroactivity [57-59]. The modified materials have not been used in SCMH fuel cell and, hence, were chosen to be used as the cathode materials for this study.

4.4.2 Material Synthesis

4.4.2.1 Hollow Fe-Fe Prussian Blue Cubes

Polyvinylpyrrolidone (PVP, MW $\approx$ 58,000) was purchased from Beantown Chemical, $K_3Fe(CN)_6$ and hydrochloric acid were purchased from Portland State University chemistry stockroom. The synthesizing method was adapted from [45]. In short, prussian blue cubes were made by, first, mixing PVP (3.0 g) with 10 mM hydrochloric acid (40 mL) for 5 minutes. Then, $K_3Fe(CN)_6$ (0.11 g) was added to the solution and stirred for another 30 minutes. Next, the mixture was aged for 20 hours at 80^o C. After 20 hours, the particles were washed with ethanol and deionized water several times and dried in vacuum overnight at 40^o C.

To create hollow porous prussian blue cubes, the solid PB cubes (20 mg) and PVP (200 mg) were added 1M HCl (20 mL) and stirred for 2 hours. Next, the mixture was heated to 140^{o}C for 4 hours. After aging, the particles was allowed to cool to room temperature before washing ethanol and DI water. Lastly, the collected material was dried in vacuum overnight at 50^{o}C.

4.4.2.2 Fe/Fe_3C Nanoparticles

Prussian blue was purchased from Sigma Aldrich. To create porous Fe/Fe_3C nanoparticles, the purchased prussian blue powder was heated to 850^o C under nitrogen gas for 2 hours, then allowed to cool to room temperature. The overall reaction of the decomposition is [44]:

$$Fe_4[Fe(CN)_6]_3 \cdot 4H_2O \rightarrow 4Fe + 5(CN)_{(2)} + 7C + 4N_2 + 4H_2O + Fe_3C \qquad (4.1)$$

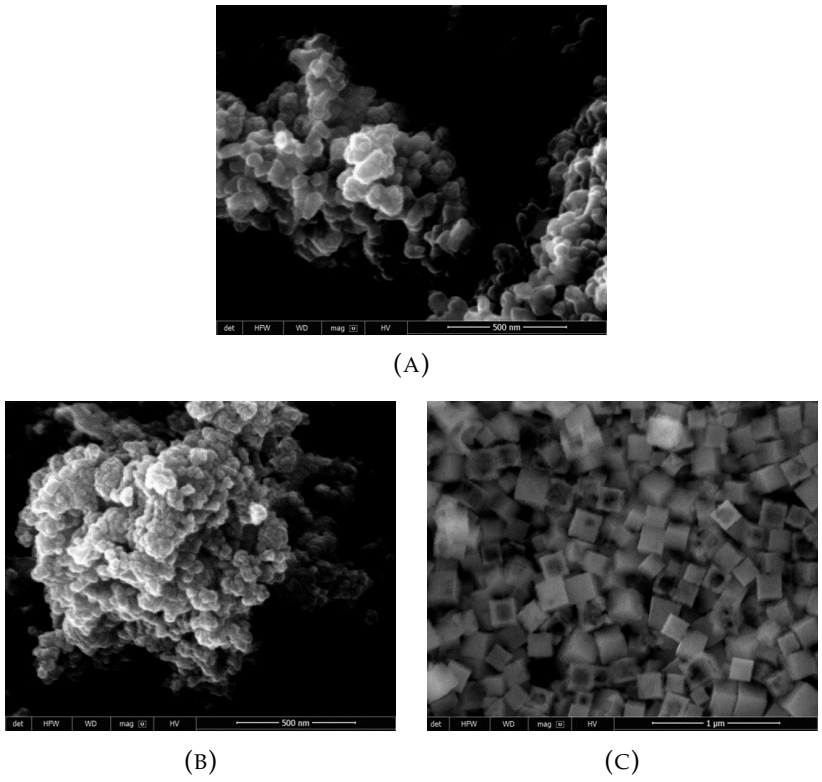

(A)

(B) (C)

FIGURE 4.8: SEM images of (A) Prussian blue as purchased, (B) porous Fe/Fe_3C particles and (C) Co-Fe prussian blue porous cubes.

4.4.3 Electrode Preparations

Electrode preparation methods were similar to the methods in MPC electrodes.

4.4.4 Results

Shaegh et al. reported 0.6 V to be the onset potential for H_2O_2 reduction on prussian blue electrode in equivolume of 0.1 M HCl and 0.5 M H_2O_2. Polarization curves for prussian blue, hollow porous Co-Fe prussian blue and Fe/Fe_3C

nanoparticles are shown in Figure 4.9. The OCP for prussian blue, prussian blue cubes and Fe/Fe_3C are 0.53 V, 0.68 V and 0.56 V, respectively. Also, the power densities are 1.20 $mW{\cdot}cm^{-2}$, 1.00 $mW{\cdot}cm^{-2}$, 2.60 $mW{\cdot}cm^{-2}$ for prussian blue, hollow porous prussian blue and Fe/Fe_3C nanoparticles, respectively. For prussian blue-nickel hydrogen peroxide fuel cell, Shaegh et al. [46] reported an OCP of 0.6V and a power density of 1.55 $mW{\cdot}cm^{-2}$ which are 0.07 V and 0.35 $mW{\cdot}cm^{-2}$ higher than the results from this study. The differences were likely due to the cathode compositions and the cell setups. The hollow porous Co-Fe prussian blue, while having the highest OCP of the three materials, has the lowest power density.

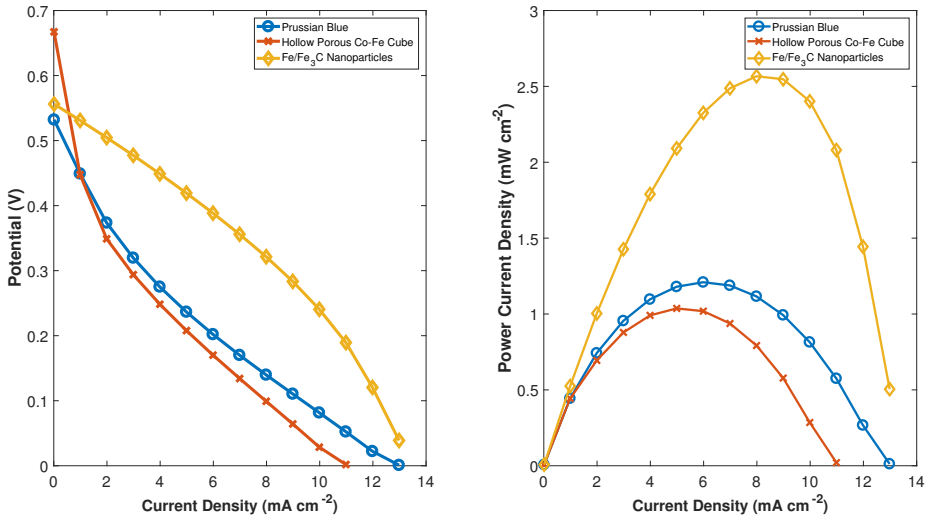

FIGURE 4.9: Polarization results for prussian blue and Fe/Fe_3C nanoparticle with nickel anode fuel cells.

The electrochemical impedance spectrograms for the three fuel cells are shown

in Figure 4.10. Gamry Echem Analyst software was used to fit the data to determine the impedance values of the modeled circuit elements. For the frequency range of the experiments, the Warburg lines did not appear, and hence, the fits were performed without the Warburg element. Table 4.2 shows the fitting results. Fe/Fe_3C fuel cell has the lowest total resistance of the three fuel cells. As mentioned in Section 3.4, the capacitance value of the double layer is related to surface area of an electrode. From the results, the capacitances of Fe/Fe_3C and porous Co-Fe cube electrodes are a magnitude larger than the prussian blue electrode which suggested that their surface areas are higher than the prussian blue electrode. The low power nature of the porous Co-Fe cube fuel cell is likely due to low permeability. Porous materials may exhibit low permeability if the pores are closed or not connected [15].

	Cathode Resistance (Ω)	Anode Resistance (Ω)	Total Resistance (Ω)	Cathode Capacitance (mF)	Anode Capacitance (μF)
Prussian blue	165.7	8.378	182.1	6.70	195
Porous Co-Fe Cubes	140.9	31.17	188.9	20.60	742.0
Fe/Fe_3C	4.48	3.489	19.93	25.40	162

TABLE 4.2: A summary of EIS fitting results for prussian blue, porous prussian blue cube and Fe/Fe_3C experiments. Different equivalent circuit models were used for the fittings. Models with the lowest goodness fit values and error values for the components were reported. Gamry software parallel resistance was used to calculated the capacitances.

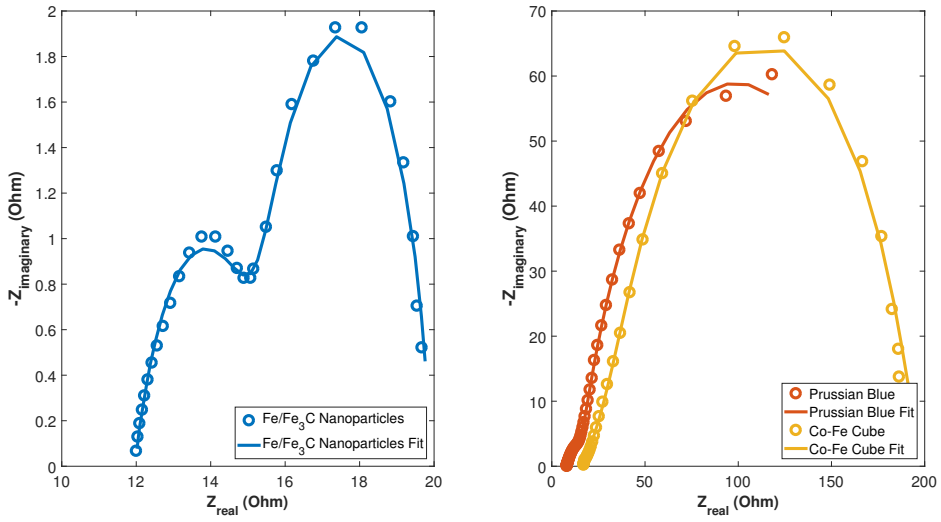

FIGURE 4.10: EIS for PB. Fe/Fe_3C cell's resistance, on the left, is a magnitude lower than the prussian blue and the hollow porous Co-Fe prussian blue fuel cells, hence, it was placed on a separate plot.

Chapter 5

Conclusions and future work

5.1 Conclusions

In this thesis, single compartment membraneless hydrogen peroxide fuel cell was studied as a potential solar energy converter to combat climate change. Different catalytic materials for hydrogen peroxide were studied and used in the fuel cells. To summarize:

- For metallophthalocyanine (FePc, CoPc, and CuPc) and iron nitride ($Fe_{x=2,3}N$) fuel cells:
  - Using cyclic voltammetry, it was found that the onset potential of H_2O_2 reduction on $Fe_{x=2,3}N$, FePc, CoPc, and CuPc were 0.57 V, 0.56 V, 0.42 V, and 0.51 V, respectively. Hence, nickel mesh was chosen to be the anode material for the fuel cells.
  - Using nickel mesh as the anode material, the polarization results showed the open circuit potential for $Fe_{x=2,3}N$, FePc, CoPc, and CuPc were 0.58 V, 0.56 V, 0.48 V, and 0.57V, respectively. The power densities, in the same order, were 0.76 $mW{\cdot}cm^{-2}$, 2.8 $mW{\cdot}cm^{-2}$, 0.28 $mW{\cdot}cm^{-2}$,

and 0.76 mW·cm^{-2}, respectively. FePc cathode with nickel mesh produced the highest output power density compared to the materials in this series.

  - The EIS results revealed that FePc fuel cell had the lowest total resistance, 12.8 Ω, and highest cathode capacitance, 2.35 x 10^3 mF. While $Fe_{x=2,3}N$ fuel cell had the second highest total resistance, 3.22 x $10^3\Omega$, the cathode capacitance was a magnitude higher, 33.2 mF, compared to CoPc and CuPc fuel cells.

- For vitamin B12 fuel cells:

  - Two different electrode preparation methods were used to address the stability issue of vitamin B12 in acidic environment.

  - The polarization results showed that while having the same OCP of about 0.48 V, the power density of the paste-method Vitamin B12 fuel cell was 0.18 mW·cm^{-2} which was 2.5 times higher than the ink-method.

  - In both fuel cells, the cathode materials immediately began to dissolve when immersed in the electrolytes. This concluded that the preparation methods did not resolve the issue of vitamin B12 dissolving in acidic environments.

- For prussian blue, prussian blue cube, and Fe/Fe_3C nanoparticle fuel cells:

  - The polarization results showed that the OCP for the PB, PB cube, and Fe/Fe_3C nanoparticle fuel cells were 0.53 V, 0.68 V, and 0.56 V,

respectively. The output power densities, in the same order, for the fuel cells were 1.55 $mW \cdot cm^{-2}$, 1.00 $mW \cdot cm^{-2}$, and 2.60 $mW \cdot cm^{-2}$. The power density of the Fe/Fe_3C fuel cell was 2 times higher than the PB fuel cell's power density in this study and 1.7 times higher than what was reported for PB fuel cell.

– The EIS results showed that Fe/Fe_3C fuel cell total resistance (19.93 Ω) was a magnitude lower than the other two fuel cells. The total resistances of PB and PB cube fuel cells were similar, but the cathode capacitance of PB cube fuel cell was a magnitude higher. Since capacitance of an electrode is proportional to the surface area of the electrode, its suggests that low permeability was the main reason for the low power output density in PB cube fuel cell.

5.2 Future Work

Further tests and experiments are required to deepen the understanding of the materials' characteristics. Till now, only electrochemical techniques are used to characterize the cathode materials and the fuel cell systems. These techniques alone cannot be used to explain why certain materials outperformed the others. For example, the porous PB cube cathode, with high surface area, was expected to perform better than the unaltered PB; the polarization results showed otherwise. While the EIS results suggested that low permeability might be the issue, more rigorous techniques are required for quantitative confirmation. So for the future work:

- Using ex situ characterization techniques to rigorously determine the structure of the catalytic materials and the chemistry of the fuel cell systems.
- Vitamin B12 has been shown to be a promising material for SCMHFC. Hence, it will be worthwhile to determine how to overcome the stability issues in acidic environments. As a start, Bhat et al. has shown that Vitamin B12 functionalized N-doped graphene is stable in acidic environment. The material has not been used in SCMHFC.
- The effects of H_2O_2 concentration and the distance between the electrodes have not been examined. An insight to these parameters could explain the difference observed between the results of PB fuel cells in literature and the results in this thesis.
- The long term stability of the fuel cells has not been examined. This can be done using chronoamperometry or chronopotentiometry.
- Lastly, while stacked SCMHFC was assembled in this thesis for demonstration purposes, it has not been studied in-depth to determine potential shortcomings.

Bibliography

[1] *NOAA Resource Collection*. Aug. 2020.

[2] Thomas E. Lovejoy, Lee Jay Hannah, and Edward O. Wilson. *Biodiversity And Climate Change*. New Haven: Yale University Press, 2019.

[3] Hibiba Gitay et al. *Climate Change and Biodiversity*. Tech. rep. New York NY, 2002.

[4] Rebecca Lindsey. *Climate Change: Atmospheric Carbon Dioxide*. Aug. 2020.

[5] Larry LeDoux. *Does Population Growth Impact Climate Change?* Ed. by Scientific American. July 2009.

[6] C Liousse et al. "Explosive growth in African combustion emissions from 2005 to 2030". In: *Environmental Research Letters* 9.3 (2014), p. 035003.

[7] Wei Li, Qingxiang Ou, and Yulu Chen. "Decomposition of China's CO_2 emissions from agriculture utilizing an improved Kaya identity". In: *Environmental Science and Pollution Research* 21 (2014), pp. 13000–13006.

[8] Joseph Chamie. *World Population: 2020 Overview*. yaleglobal.yale.edu/content/world-population-2020-overview. Feb. 2020.

[9] D. Abbott. "Keeping the Energy Debate Clean: How Do We Supply the World's Energy Needs?" In: *Proceedings of the IEEE* 98.1 (2010), pp. 42–66.

[10] Energy Information AdministrationEIA. *World Energy Outlook 2019*. Technical Report. 2019. URL: https://www.eia.gov/outlooks/ieo/pdf/ieo2019.pdf.

[11] *NASA Science SpacePlace*. Aug. 2020.

[12] Yu Hou, Ruxandra Vidu, and Pieter Stroeve. "Solar Energy Storage Methods". In: *Industrial & Engineering Chemistry Research* 50.15 (2011), pp. 8954–8964. DOI: 10.1021/ie2003413. eprint: https://doi.org/10.1021/ie2003413. URL: https://doi.org/10.1021/ie2003413.

[13] Scott A. Gold. "Low-Temperature Fuel Cell Technology for Green Energy". In: *Handbook of Climate Change Mitigation and Adaptation*. Ed. by Wei-Yin Chen, Toshio Suzuki, and Maximilian Lackner. Cham: Springer International Publishing, 2017, pp. 3039–3085.

[14] Norazlianie Sazali et al. "New Perspectives on Fuel Cell Technology: A Brief Review". In: *Membranes* 10.5 (2020).

[15] Ryan O' Hayre et al. *Fuel Cell Fundamentals*. 3rd. New Jersey: Wiley, 2016.

[16] Cordelia Sealy. "The problem with platinum". In: *Materials Today* 11.12 (2008), pp. 65–68. ISSN: 1369-7021.

[17] Sajad Ahmad Bhat et al. "Vitamin B12 functionalized N-Doped graphene: A promising electro-catalyst for hydrogen evolution and electro-oxidative sensing of H2O2". In: *Electrochimica Acta* 337 (2020), p. 135730.

[18] *Comparison of Fuel Cell Technologies*. https://www.energy.gov/eere/fuelcells/comparison-fuel-cell-technologies. Accessed: 2020-10-30.

[19] Yusuke Yamada, Masaki Yoneda, and Shunichi Fukuzumi. "A Robust One-Compartment Fuel Cell with a Polynuclear Cyanide Complex as a Cathode for Utilizing H2O2 as a Sustainable Fuel at Ambient Conditions". In: *Chemistry Europe* 19(5) (35 2013), pp. 11733–11741.

[20] Seyed Ali Mousavi Shaegh et al. "A membraneless hydrogen peroxide fuel cell using Prussian Blue as cathode material". In: *Energy Environ. Sci.* 5 (8 2012), pp. 8225–8228. DOI: 10.1039/C2EE21806B. URL: http://dx.doi.org/10.1039/C2EE21806B.

[21] Robert S. Disselkamp. "Energy Storage using Aqueous Hydrogen Peroxide". In: *Energy & Fuels* 22.4 (2008), pp. 2771–2774.

[22] Satoshi Kato et al. "Production of hydrogen peroxide as a sustainable solar fuel from water and dioxygen". In: *Energy Environ. Sci.* 6 (12 2013), pp. 3756–3764.

[23] Kentaro Mase et al. "Seawater usable for production and consumption of hydrogen peroxide as a solar fuel". In: *Energy Environ. Sci.* 5 (8 2012), pp. 8225–8228. DOI: 10.1039/C2EE21806B. URL: http://dx.doi.org/10.1039/C2EE21806B.

[24] Jiali Liu et al. "Hydrogen Peroxide Production from Solar Water Oxidation". In: *ACS Energy Letters* 4.12 (2019), pp. 3018–3027.

[25] Allen J. Bard and Larry R. Faulkner. *Electrochemical methods: fundamentals and applications*. New York: Wiley, 1980.

[26] Noémie Elgrishi et al. "A Practical Beginner's Guide to Cyclic Voltammetry". In: *Journal of Chemical Education* 95.2 (Nov. 2017). DOI: 10.1021/acs.jchemed.7b00361.

[27] Woosung Choi et al. "Modeling and Applications of Electrochemical Impedance Spectroscopy (EIS) for Lithium-ion Batteries". In: *J. Electrochem. Sci. Technol* 11.1 (2020), pp. 1–13. DOI: 10.33961/jecst.2019.00528. URL: http://www.jecst.org/journal/view.php?number=315.

[28] V.D. Jovic. *Determination of the correct value of Cdl from the impedance results fitted by the commercially available software*. Available at https://www.gamry.com/assets/Application-Notes/Determination-of-Double-Layer-Capacitance-from-a-CPE.pdf (2005/06/12).

[29] P.R. Ortiz de Montellano. *Cytochrome P-450: Structure, Mechanism and Biochemistry*. 5th ed. New York: Kluwer Academic/Plenum Publishers, 2005.

[30] Pui-Chi Lo, Xuebing Leng, and Dennis K.P. Ng. "Hetero-arrays of porphyrins and phthalocyanines". In: *Coordination Chemistry Reviews* 251 (2007), pp. 2334–2353.

[31] Alexander B. Sorokin. "Phthalocyanine Metal Complexes in Catalysis". In: *American Chemical Society* 113(10) (2013), pp. 8152–8191.

[32] Christian G. Claessens, Uwe Hahn, and Tomas Torres. "Phthalocyanines: From Outstanding Electronic Properties to Emerging Applications". In: *Chemical Record* 8(2) (2008), pp. 75–97.

[33] Mårten Wikström et al. "New Perspectives on Proton Pumping in Cellular Respiration". In: *Chemical Reviews* 115.5 (2015), pp. 2196–2221.

[34] Shelagh Ferguson-Miller and Gerald T. Babcock. "Heme/Copper Terminal Oxidases". In: *Chemical Reviews* 96.7 (1996), pp. 2889–2908.

[35] Wei Chen et al. "Recent advances in electrochemical sensing for hydrogen peroxide: a review". In: *Analyst* 137 (1 2012), pp. 49–58.

[36] Douglas B. Young, Iñaki Comas, and Luiz P. S. de Carvalho. "Phylogenetic analysis of vitamin B12-related metabolism in Mycobacterium tuberculosis". In: *Frontiers in Molecular Biosciences* 2 (2015), p. 6.

[37] Alexander Kraft. "What a chemistry student should know about the history of Prussian blue". In: *ChemTexts* 4(4) (2018), pp. 1–11.

[38] *What is Prussian blue*. Accessed: 2010-12-27. URL: https://www.cdc.gov/nceh/radiation/emergencies/prussianblue.htm.

[39] J. F Duncan and P.W.R Wigley. "The electronic structure of the iron atoms in complex iron cyanides". In: *Journal of the Chemical Society* (1963), p. 1120.

[40] Alexander Kraft, Matthias Rottmann, and Karl-Heinz Heckner. "Large-area electrochromic glazing with ion-conducting PVB interlayer and two complementary electrodeposited electrochromic layers". In: *Solar Energy Materials and Solar Cells* 90 (2006), pp. 69–476.

[41] Vernon D. Neff. "Some Performance Characteristics of a Prussian Blue Battery". In: *Journal of The Electrochemical Society* 132.6 (1985), pp. 1382–1384.

[42] Kingo Itaya, Nobuyoshi Shoji, and Isamu Uchida. "Catalysis of the reduction of molecular oxygen to water at Prussian blue modified electrodes". In: *Journal of the American Chemical Society* 106.12 (1984), pp. 3423–3429.

[43] Arkady A. Karyakin, Olga V. Gitelmacher, and Elena E. Karyakina. "Prussian Blue-Based First-Generation Biosensor. A Sensitive Amperometric Electrode for Glucose". In: *Analytical Chemistry* 67.14 (1995), pp. 2419–2423.

[44] Ankit Kumar et al. "Supercapacitors with Prussian Blue Derived Carbon Encapsulated Fe/Fe3C Nanocomposites". In: *Journal of The Electrochemical Society* 167.6 (2020), p. 060529.

[45] Qinglin Sheng et al. "Synthesis of hollow Prussian blue cubes as an electrocatalyst for the reduction of hydrogen peroxide". In: *Frontiers of Materials Science* 11.2 (June 2017), pp. 147–154. DOI: 10.1007/s11706-017-0382-z.

[46] Seyed Ali Mousavi Shaegh et al. "A membraneless hydrogen peroxide fuel cell using Prussian Blue as cathode material". In: *Energy Environ. Sci.* 5 (8 2012), pp. 8225–8228.